Journal of Power Sources 195 (2010) 3612–3620

Contents lists available at ScienceDirect

Journal of Power Sources

journal homepage: www.elsevier.com/locate/jpowsour

Mechanical behavior and electrical conductivity of $La_{1-x}Ca_xCoO_3$ ($x = 0, 0.2, 0.4, 0.55$) perovskites

Siddhartha Pathak[a,1], Jakob Kuebler[b], Andrew Payzant[c], Nina Orlovskaya[d,*]

[a] Department of Materials Science and Engineering, Drexel University, 3141 Chestnut Street, LeBow 344, Philadelphia, PA 19104, USA
[b] Empa, Materials Science and Technology, Laboratory for High Performance Ceramics, Ueberlandstrasse 129, CH-8600 Duebendorf, Switzerland
[c] Materials Science and Technology Division, Oak Ridge National Laboratory, 1 Bethel Valley Road, PO Box 2008, MS 6064, Building 4515, Room 113, Oak Ridge, TN, 37831-6064, USA
[d] Department of Mechanical, Materials, and Aerospace Engineering, University of Central Florida, 4000 Central Florida Blvd, Orlando, FL 32816, USA

ARTICLE INFO

Article history:
Received 7 October 2009
Received in revised form
27 November 2009
Accepted 27 November 2009
Available online 3 December 2009

Keywords:
Perovskite
Modulus
Bending strength
Fracture toughness
Ferroelasticity
Conductivity

ABSTRACT

This paper compares the important mechanical properties and the electrical conductivities from room temperature to 800 °C of four $LaCoO_3$ based cobaltite compositions with 0, 20, 40 and 55% Ca^{2+} ions substituted on the A site of the perovskite structure respectively. Ca^{2+} doped lanthanum cobaltite materials are strong candidates for use as cathodes in lower temperature solid oxide fuel cells operating at or below 800 °C. Among these four cobaltite compositions, two ($LaCoO_3$ and $La_{0.8}Ca_{0.2}CoO_3$) were found to be phase pure materials, whereas the remaining two compositions ($La_{0.6}Ca_{0.4}CoO_3$ and $La_{0.45}Ca_{0.55}CoO_3$) contained precipitation of secondary phases such as CaO and Co_3O_4. The mechanical properties of the four compositions, in terms of Young's modulus, four-point bending strength and fracture toughness measurements, were measured at both room temperature and 800 °C. At room temperature, doping with Ca^{2+} was found to substantially increase the mechanical properties of the cobaltites, whereas at 800 °C the pure $LaCoO_3$ composition exhibited higher modulus and strength values than $La_{0.8}Ca_{0.2}CoO_3$. All of the four compositions exhibited ferroelastic behavior, as shown by the hysteresis loops generated during uniaxial load–unload compression tests. Electrical conductivity measurements showed the $La_{0.8}Ca_{0.2}CoO_3$ composition to have the highest conductivity among the four compositions.

1. Introduction

As mixed ionic-electronic conductors (MIEC), lanthanum cobaltite ($LaCoO_3$) based perovskite ceramics are attractive candidates for cathodes in intermediate temperature (600–800 °C) solid oxide fuel cells (IT-SOFCs) [1] and for high temperature oxygen separation membranes [2], due to their high electronic and ionic conductivity, as well as their good catalytic activity [3]. However, the relatively poor mechanical properties of the cobaltites have resulted in their limited use in these applications. For example, the coefficient of thermal expansion for cobaltites (about $25 \times 10^{-6}\,K^{-1}$) [4] is much higher than that of Yttria Stabilized Zirconia (YSZ, $10.5 \times 10^{-6}\,K^{-1}$), which results in high thermally induced mechanical stresses when used in SOFCs [5]. During fabrication and operation, these large thermal stresses can cause cracking and failure of the SOFC's components [6]. $LaCoO_3$ based oxygen separation membranes also experience severe mechanical stresses arising due to differential thermal expansion which can cause the membranes to fracture [2]. Thus, for such high temperature applications, a better understanding of the mechanical properties and reliability of the $LaCoO_3$ based perovskites is very important.

Pure $LaCoO_3$ is reported to have a $R\bar{3}c$ rhombohedral structure, as determined by X-ray diffraction (XRD), which remains rhombohedral up to temperatures well above 1000 °C [7,8]. The rhombohedral distortion of $LaCoO_3$ based perovskites decreases with increasing temperature and increasing divalent cation substitution on the A site [9,10]. At 50 mol% substitution lanthanum with strontium, the crystal structure becomes cubic [9,11]. At moderate substitution levels with calcium or strontium ($x = 0.2$), however, the rhombohedral distortion remains significant at room temperature. The rhombohedral to cubic phase transition is observed at ~900 °C for the 20 mol% Ca substituted materials [12]. Ca is reported to have a limited solid solubility in the perovskite structure. Thus, while the formation of single perovskite phase has been reported for the compositions with up to 28 mol% Ca dop-

* Corresponding author. Tel.: +1 407 823 5770; fax: +1 407 823 0208.
E-mail addresses: sp324@drexel.edu (S. Pathak), Jakob.Kuebler@empa.ch (J. Kuebler), payzanta@ornl.gov (A. Payzant), norlovsk@mail.ucf.edu (N. Orlovskaya).
[1] Present address: Empa, Swiss Federal Laboratory for Materials Testing and Research, Feuerwerkerstrasse 39, CH-3602 Thun, Switzerland.

0378-7753/$ – see front matter © 2009 Elsevier B.V. All rights reserved.
doi:10.1016/j.jpowsour.2009.11.134

ing on the A site, the formation of secondary phases such as CaO, CoO and Co_3O_4, has been observed for 30 and higher mol% of Ca substitution [13]. A local *I*2/*a* monoclinic distortion in $LaCoO_3$, that cannot be detected by XRD, has been reported in [14–17]. Spin state transitions are another characteristic feature of the cobaltites [18]. $LaCoO_3$ also shows a semiconductor to metal transition with increasing temperature [19,20]. At ambient temperature pure $LaCoO_3$ is a semiconductor, but becomes a metallic oxide with increasing temperature or when lanthanum is substituted by alkali earth cations [10,21].

Despite the fact that high temperature application of these materials demands a certain level of mechanical properties, there are only a few reports in the literature on this subject [6,8,22,23]. The mechanical properties of $LaCoO_3$, $La_{0.8}Sr_{0.2}CoO_3$ and $La_{0.8}Ca_{0.2}CoO_3$ perovskites have been studied in [23] where the four-point bending strength was found to be 53 MPa for 83% dense $LaCoO_3$, 76 MPa for 90% dense $La_{0.8}Sr_{0.2}CoO_3$, and 151 MPa for fully dense (>99%) $La_{0.8}Ca_{0.2}CoO_3$ ceramic at room temperature. The strengths of $LaCoO_3$ and $La_{0.8}Sr_{0.2}CoO_3$ were relatively independent of temperature up to 850 °C while that of $La_{0.8}Ca_{0.2}CoO_3$ was found to decrease with increasing temperatures (~100 MPa at 600 °C and ~70 MPa at 850 °C). The fracture toughness, measured by indentation, was found to be 0.73 MPa $m^{1/2}$ for 90% dense $La_{0.8}Sr_{0.2}CoO_3$ and 0.98 MPa $m^{1/2}$ for fully dense $La_{0.8}Ca_{0.2}CoO_3$ ceramics. In another work [6], fracture toughness at room temperature, using the single edge V notch beam (SEVNB) method, of $La_{0.8}Ca_{0.2}CoO_3$ ceramics was reported to be about twice as high as the fracture toughness of pure $LaCoO_3$ (2.25 and 1.32 MPa $m^{1/2}$, respectively). A nonlinear deformation was observed during the flexure strength measurements on all three $LaCoO_3$ based perovskites [23]. Cobaltites are known to exhibit a ferroelastic hysteretic behavior and this phenomenon has been demonstrated in various experiments, such as four-point bending, compression and indentation tests [6,8,22].

The aim of the present study was therefore to conduct a further investigation into the mechanical properties of $LaCoO_3$ based perovskites. Four different compositions, $LaCoO_3$, $La_{0.8}Ca_{0.2}CoO_3$, $La_{0.6}Ca_{0.4}CoO_3$ and $La_{0.45}Ca_{0.55}CoO_3$, were studied in this work with respect to their phase composition, elastic modulus, bending strengths, fracture toughness and stress–strain behavior under compression – both at room and high temperatures. The electrical conductivities of the four compositions as a function of temperature are also reported.

2. Experimental procedure

Sintered bars of $LaCoO_3$, $La_{0.8}Ca_{0.2}CoO_3$, $La_{0.6}Ca_{0.4}CoO_3$ and $La_{0.45}Ca_{0.55}CoO_3$ were produced by Praxair Surface Technologies, Specialty Ceramics, USA. After sintering, the bars were machined to 2.5 mm × 4 mm × 50 mm size. The bulk density of all the machined specimens was measured by Archimedes method [24]. The density of the machined specimens was also measured using the Helium Pycnometer, AccuPyc 1330 (Micromerities Instrument Corporation, GA, USA). The theoretical density was calculated using the technique described in [25]. The porosity in the samples was then estimated from the difference between the values of theoretical and bulk density.

X-ray powder diffraction (XRD) of the crushed bar samples was carried out on a Scintag PADV diffractometer (Cu Kα radiation) in 20–55° 2θ range with 0.02° angular step and collection time of 8 s per step. JADE software [Materials Data Inc., Livermore, CA, USA] was used to identify the XRD peaks in the material.

The Young's modulus (E) was measured using three different methods, namely impulse excitation (natural frequency), 4-point bending and compression loading. In the impulse excitation method [26] the Young's modulus was measured both at room and high temperatures using a Grindo–Sonic MK 5 (Lemmens, Belgium) in accordance with the ASTM EN 843-2 standard. The sample with a known density was placed over the microphone lining up with the supporting cylinders. The sample was then struck with a small hammer and the resulting frequency was recorded by the MK5 machine. The test setup and procedure were modified for measuring the Young's modulus by impulse excitation method at elevated temperatures. For high temperature experiments, the specimens were hung and fixed with very fine platinum wires in a small oven. Then a thin ceramic pipe was lined up with the sample and connected outside the oven to the microphone. A second ceramic pipe was placed above the sample with one end outside the oven. The samples were heated up with a rate of 15 °C min^{-1} in air and after reaching a specific temperature the samples were equilibrated for about 10 min. Finally, the natural frequency of the sample was activated by hitting it with a small ceramic ball using the 2nd pipe as a drop guide.

The Young's modulus at room temperature was also calculated as the secant modulus up to a stress of 9 MPa from stress–strain curves that were obtained in 4-point bending tests using a 40/20 mm load geometry at a cross-head displacement speed of 0.4 mm min^{-1} (Universal Testing Machine UPM-Zwick 1478, Germany). Deflection of the specimen during loading and unloading was measured with the help of three pushrods. The two outer pushrods were spaced at a distance of 20 mm to correspond with the location of the upper (=inner) two rollers of the bend fixture. The middle rod was placed midway between the two outer rods. The deflection of the specimen was measured as the relative deflection of the centre pushrod with respect to the outer rods. As a third comparison, the secant modulus in the range of 0–9 MPa was calculated from stress–strain curve that were determined from uniaxial compression tests at room temperature. The uniaxial compression tests were performed on cylindrical samples (6 mm in diameter and 12 mm height) in a servohydraulic test machine (Instron 8511) with a 20 kN load cell under load control with a loading rate of 3 MPa s^{-1}. The compression load was applied along the height of the cylinders. The axial strain was measured using three strain gauges mounted on the surface of each sample. The total strain was determined by averaging the signals from the three strain gauges.

Four-point bending strength was also measured using a 40/20 mm load geometry. The tests were carried out at room temperature with a cross-head displacement speed of 1 mm min^{-1} (UTM, Zwick Z005, Germany) and at 800 °C with a cross-head displacement speed of 0.1 mm min^{-1} (Universal Testing Machine UPM-Zwick 1478, Germany) in accordance to ASTM EN 843-1 [27]. At each temperature, 5 samples were tested to failure.

Fracture toughness (K_{Ic}) was measured using the single edge V notch beam (SEVNB) method [27]. The notches were inserted using a specifically constructed notching machine and the final notching was performed using 1 μm diamond paste and a steel razor blade. The K_{Ic} values were measured at room temperature, 700 and 800 °C in air. The cross-head displacement speed was 0.3 mm min^{-1} for room temperature experiments (UTM, Zwick Z005, Germany) and 0.1 mm min^{-1} for high temperature measurements (Universal Testing Machine UPM-Zwick 1478, Germany). Three specimens of each composition were tested at each temperature. Fractographic analysis was carried out on selected specimens using both optical microscopy and scanning electron microscopy (Tescan Vega Plus 5136 MM).

The conductivity of the samples was measured with a Resistomat 2318 (Burster, Switzerland) up to temperatures of 900 °C according to the procedure outlined in ASTM F 43-93 (4 probe method) [28]. One specimen of each composition was chosen for conductivity measurements with a heating rate of 150 °C h^{-1} and a hold time of 30 min at each measured temperature.

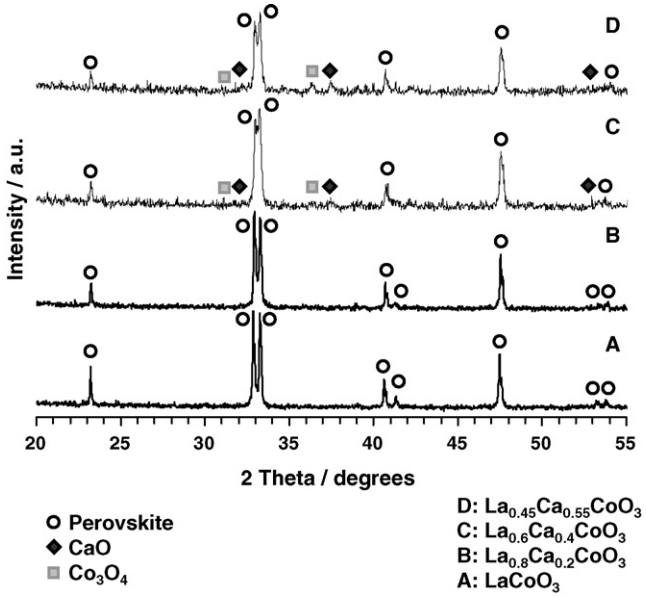

Fig. 1. XRD of undoped $LaCoO_3$, $La_{0.8}Ca_{0.2}CoO_3$, $La_{0.6}Ca_{0.4}CoO_3$ and $La_{0.45}Ca_{0.55}CoO_3$.

3. Results and discussion

3.1. Phase composition and porosity

XRD analysis (see Fig. 1) of $LaCoO_3$, $La_{0.8}Ca_{0.2}CoO_3$, $La_{0.6}Ca_{0.4}CoO_3$ and $La_{0.45}Ca_{0.55}CoO_3$ shows that $LaCoO_3$ and $La_{0.8}Ca_{0.2}CoO_3$ have single phase rhombohedral ($R\bar{3}c$) structure. The two other compositions, $La_{0.6}Ca_{0.4}CoO_3$ and $La_{0.45}Ca_{0.55}CoO_3$, show presence of secondary phases – CaO and Co_3O_4. While significant amounts of these secondary phases were detected in $La_{0.45}Ca_{0.55}CoO_3$, only trace amounts were found in $La_{0.6}Ca_{0.4}CoO_3$. The presence of the secondary phases is further corroborated by the backscattered electron microscopy (BSE) at room temperature. As can be seen from Fig. 2, there is no contrast difference in the case of $LaCoO_3$ and $La_{0.8}Ca_{0.2}CoO_3$ other than the porosity, while for the $La_{0.6}Ca_{0.4}CoO_3$ and $La_{0.45}Ca_{0.55}CoO_3$ the presence of the three different phases along with the porosity could be detected. Because of the existence of the secondary phases, the stoichiometry of these two latter compositions is obviously altered. However, for simplicity, we refer to these compositions as $La_{0.6}Ca_{0.4}CoO_3$ and $La_{0.45}Ca_{0.55}CoO_3$ in this paper in spite of the known secondary phases and non-stoichiometry.

Table 1 shows a comparison of the density/porosity between the four cobaltite compositions. Three different estimates of the density are shown. Note that the theoretical density values for the $La_{0.6}Ca_{0.4}CoO_3$ and $La_{0.45}Ca_{0.55}CoO_3$ compositions are not strictly valid because of their known non-stoichiometry. Using this approach, all of the compositions except $LaCoO_3$ were found to have low porosity values (3–5%). The $LaCoO_3$ samples showed a higher porosity of ~10%. This higher porosity of the $LaCoO_3$ sample can also be seen from the BSE images (Fig. 2a).

3.2. Young's modulus

The results of the measured Young's (E) modulus values for the four compositions are shown in Fig. 3. In this figure, the room temperature values for E in uniaxial compression, determined as the secant moduli from 0 to 9 MPa [8], are compared to the values obtained from 4-point bending and the natural frequency method. At room temperature, E determined by the natural frequency technique shows the highest average values of 76, 141, 141 and 150 GPa for the four cobaltite compositions, $LaCoO_3$, $La_{0.8}Ca_{0.2}CoO_3$, $La_{0.6}Ca_{0.4}CoO_3$, and $La_{0.45}Ca_{0.55}CoO_3$ respectively, which is expected to be the most accurate modulus value among the three techniques used in this paper [29]. The E values calculated from the bending and uniaxial compression data are generally lower, which reflect the softening of the materials due to domain wall movement during loading [8]. However, the differences between the Young's moduli measured by three different techniques are not very high.

The E modulus values for undoped $LaCoO_3$ at room temperature are much lower than the E modulus values for the other three compositions (Fig. 3). The undoped $LaCoO_3$ composition has about 10% porosity which could certainly contribute to a decrease in modulus [30–32]; however it is also expected that the Ca^{2+} doping will stiffen the ceramics, leading to a higher modulus value for the Ca doped compositions.

At high temperature (800 °C), remarkably different modulus behavior was noted for the undoped and Ca doped cobaltites ($LaCoO_3$ and $La_{0.8}Ca_{0.2}CoO_3$). While undoped $LaCoO_3$ exhibits significant stiffening upon heating – from 76 GPa at room temperature to 101 GPa at 800 °C – the opposite effect is observed for the $La_{0.8}Ca_{0.2}CoO_3$ composition, where the E modulus decreases to ~68 GPa upon heating to 800 °C. One possible reason for such behavior could be an unreported phase transition in $LaCoO_3$ in 800–1000 °C temperature range; however more thorough research needs to be conducted to determine the structure of $LaCoO_3$ in this temperature range in order to verify this hypothesis. Although no detectable structural changes were observed during XRD [8], these results are not conclusive, since for $LaCoO_3$ structure, the diffraction pattern is predominantly determined by the cation sublattice (where the electron density is much greater). Small changes in the oxygen positions or vacancies in the anion sublattice can go undetected by XRD, for which case neutron diffraction measurements may be required to resolve such changes.

3.3. Strength

The four-point bending strength data for all four cobaltite compositions at the two different temperatures (room temperature and 800 °C) is shown in Fig. 4. At room temperature, Ca doping appears to significantly increase the strength values of the cobaltites (from 72 ± 10 MPa for $LaCoO_3$ to ~180 MPa for the Ca doped cobaltites). Note that the higher porosity (~10%) of the

Table 1
Density as measured by water displacement technique (Archimedes method), by the Helium Pycnometer and the theoretical density of the four cobaltite compositions. The $LaCoO_3$ samples exhibit a significantly higher porosity than others. The Archimedes and He Pycnometer values are averages of measurements on 20 samples.

	Density – Archimedes (g cm^{-3})	Density – He Pycnometer (g cm^{-3})	Theoretical density (g cm^{-3})	Porosity
$LaCoO_3$	6.55	7.09	7.29	10.2%
$La_{0.8}Ca_{0.2}CoO_3$	6.36	6.39	6.73	5.4%
$La_{0.6}Ca_{0.4}CoO_3$	5.95	5.98	6.15	3.3[a]%
$La_{0.45}Ca_{0.55}CoO_3$	5.64	5.69	5.71	1.2[a]%

[a] Note that both $La_{0.6}Ca_{0.4}CoO_3$ and $La_{0.45}Ca_{0.55}CoO_3$ have secondary phases and are non-stoichiometric. The theoretical densities for these compositions were calculated from the theoretical densities of the pure compounds without secondary phases.

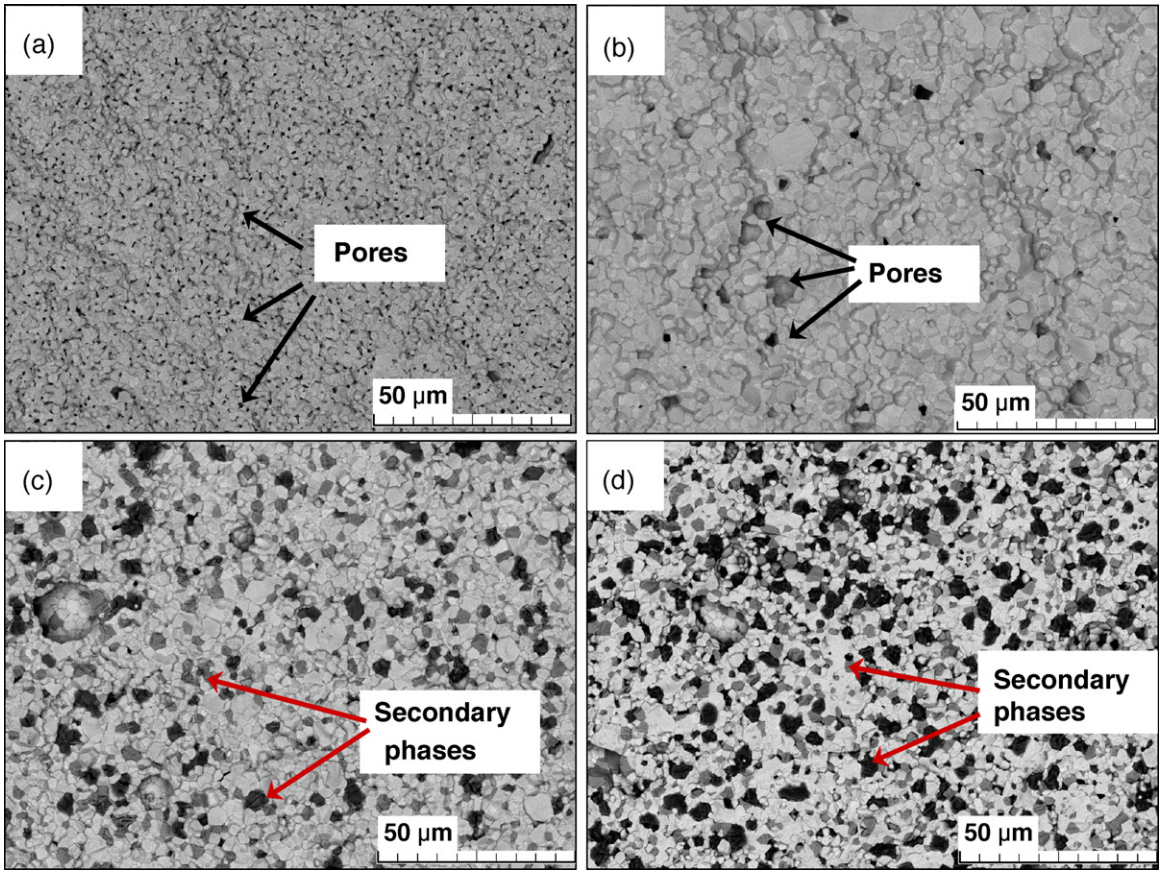

Fig. 2. BSE images of fracture surfaces produced at room temperature of (a) undoped $LaCoO_3$, (b) $La_{0.8}Ca_{0.2}CoO_3$, (c) $La_{0.6}Ca_{0.4}CoO_3$ and (d) $La_{0.45}Ca_{0.55}CoO_3$ showing presence of secondary phases in (c) and (d). Note the higher pore density in (a).

undoped $LaCoO_3$ samples could be a possible cause for the lower strengths measured in these samples. Overall, the room temperature bending strength values of the cobaltites are seen to follow a similar trend as their modulus values (see Fig. 3). Literature values of room temperature four-point bending for $LaCoO_3$ have been reported to be $\sim 53 \pm 5$ MPa for samples with 16% porosity [23], and ~65 MPa for 7% porosity [22], while that of dense $La_{0.8}Ca_{0.2}CoO_3$ were around 150 ± 20 MPa [23], all of which are comparable to our results. However, Kleveland et al. [22] have also reported the strength value of dense (2% porosity) $La_{0.8}Ca_{0.2}CoO_3$ as $\sim 111 \pm 18$ MPa which is significantly less than the values obtained in this work. Increase in temperature to 800 °C causes an increase in the bending strength values of undoped $LaCoO_3$ (from 72 ± 10 MPa at room temperature to 109 ± 19 MPa at 800 °C), and this high temperature value remains more or less constant with increase in Ca doping up to 40% Ca (91 ± 6 MPa for $La_{0.8}Ca_{0.2}CoO_3$ and 127 ± 13 MPa for $La_{0.6}Ca_{0.4}CoO_3$). A similar trend of increasing strength values with higher temperatures has been noted before in the literature [23], although the absolute strength values in that case (~50 MPa for $LaCoO_3$ and ~60 MPa for $La_{0.8}Ca_{0.2}CoO_3$ at 800 °C [23]) were much lower than the values presented in this work.

A significant increase in bending strength values for the 55% Ca doped cobaltite ($La_{0.45}Ca_{0.55}CoO_3$) at 800 °C (257 ± 33 MPa) is also noted in Fig. 4. Indeed, at this higher temperature these samples were found to behave in a highly malleable fashion (Fig. 4 inset (a)) which leads to their higher strength values. Note that this amount of plastic deformation and creep at high temperatures renders the 4-point bending strength results in this material questionable. There is a possibility that the changes in phase composition that occur in the $La_{0.45}Ca_{0.55}CoO_3$ samples during heating to 800 °C and dwelling at that temperature are responsible for this behavior. This is evidenced by the appearance of the Co_3O_4 spinel after heating and dwelling at 800 °C and subsequent cooling, whereas before heating only CoO was detected as the cobalt containing secondary phase in $La_{0.45}Ca_{0.55}CoO_3$ by XRD. This implies that some of the Co^{2+} ions were oxidized to Co^{3+} ions of the complex Co_3O_4 spinel oxide due to heating resulting in extensive plastic deformation of the samples before failure.

Fracture surfaces of the four compositions are shown in Fig. 5. Fracture origins in most of the samples are large pores or voids of ~50–100 μm size.

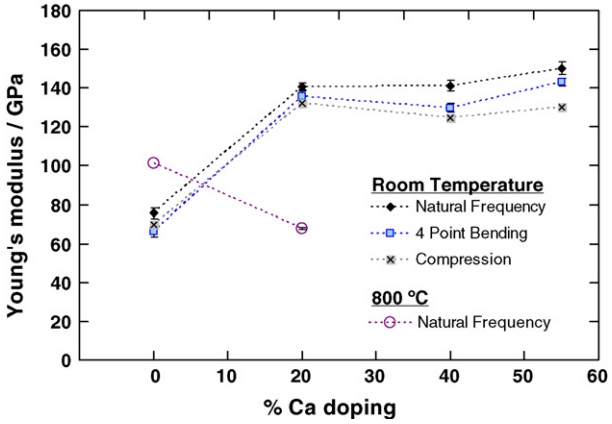

Fig. 3. Elastic modulus of the four cobaltite compositions as determined by different methods: natural frequencies, four-point bending, and uniaxial compression. The measurements at 800 °C were conducted for the $LaCoO_3$ and $La_{0.8}Ca_{0.2}CoO_3$ compositions using the natural frequency method.

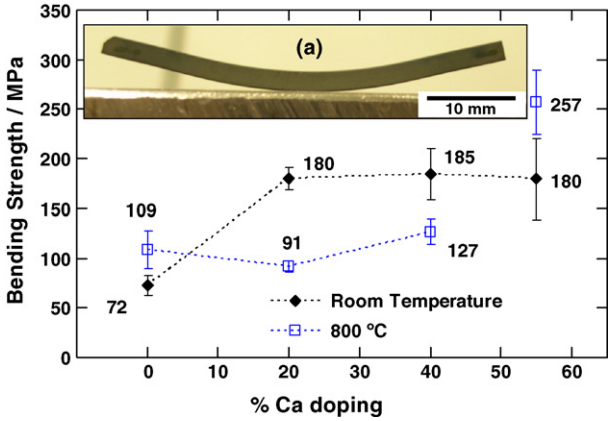

Fig. 4. The 4-point bending strength data for the cobaltites at room temperature and 800 °C as a function of Ca doping. Inset (a) ductile behavior of $La_{0.45}Ca_{0.55}CoO_3$ at 800 °C loaded in 4-point bending.

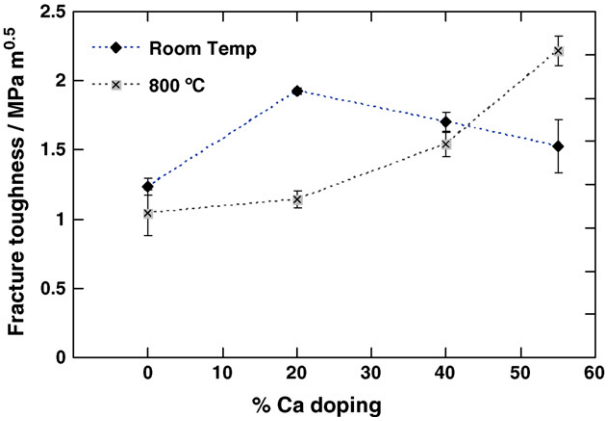

Fig. 6. Comparison of fracture toughness values for the cobaltites at room temperature and 800 °C as a function of Ca doping.

3.4. Fracture toughness

Fracture toughness values of the lanthanum cobaltites measured using the SEVNB method at room temperature and 800 °C are shown in Fig. 6. At room temperature, doping of the cobaltite with Ca raises its fracture toughness – from $1.2 \pm .06$ MPa $m^{1/2}$ for $LaCoO_3$ to $1.9 \pm .02$ MPa $m^{1/2}$ for $La_{0.8}Ca_{0.2}CoO_3$ – which remains relatively constant with increasing Ca doping (with a slight decrease for $La_{0.45}Ca_{0.55}CoO_3$ to $1.5 \pm .19$ MPa $m^{1/2}$). These values are comparable to the ones reported in the literature at room temperature for $LaCoO_3$ (1.32 MPa $m^{1/2}$ [6] and 1.3 MPa $m^{1/2}$ [22]) and for $La_{0.8}Ca_{0.2}CoO_3$ (2.25 MPa $m^{1/2}$ [6] and 2.2 MPa $m^{1/2}$ [22]). The higher K_{Ic} values of the Ca doped cobaltites at room temperature is probably related to their higher Young's modulus (Fig. 3) as well as to the larger hysteresis loop area observed in these perovskites, where much larger energy absorption occurs during deformation leading to the increase in the fracture toughness in Ca doped cobaltites [8] than those measured for pure $LaCoO_3$ (discussed later in Fig. 8). The fracture toughness values for $LaCoO_3$ at 800 °C ($1.05 \pm .16$ MPa $m^{1/2}$) are mostly unchanged with a slight decrease from their room temperature measurements, while that of $La_{0.8}Ca_{0.2}CoO_3$ ($1.14 \pm .06$ MPa $m^{1/2}$) and $La_{0.6}Ca_{0.4}CoO_3$ ($1.54 \pm .09$ MPa $m^{1/2}$) are lower than their room

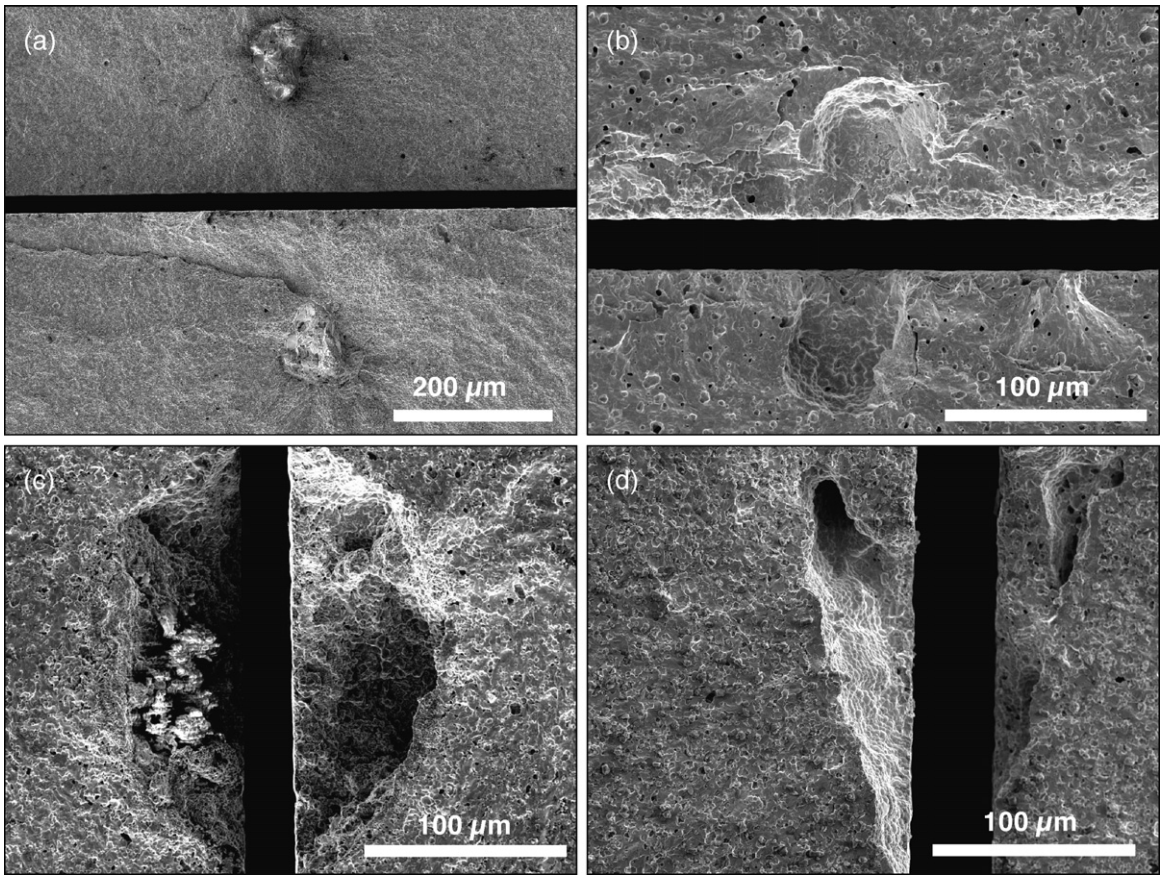

Fig. 5. Examples of typical fracture origins in 4-point bending at room temperature for (a) undoped $LaCoO_3$, (b) $La_{0.8}Ca_{0.2}CoO_3$, (c) $La_{0.6}Ca_{0.4}CoO_3$ and (d) $La_{0.45}Ca_{0.55}CoO_3$. Note the lower magnification in (a).

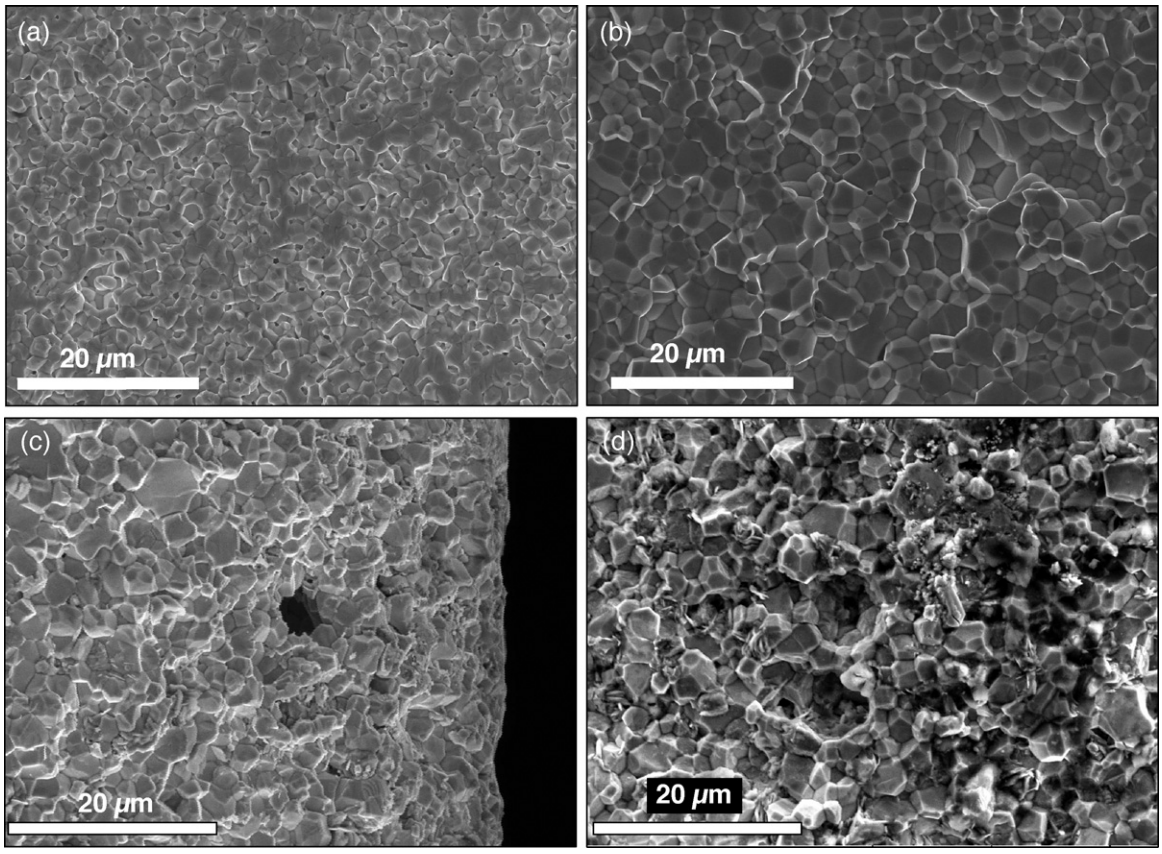

Fig. 7. Fracture surfaces during K_{Ic} testing at 800 °C for (a) undoped $LaCoO_3$, (b) $La_{0.8}Ca_{0.2}CoO_3$, (c) $La_{0.6}Ca_{0.4}CoO_3$ and (d) $La_{0.45}Ca_{0.55}CoO_3$.

temperature values. Again the trend at higher temperature is seen to reflect the Young's modulus values at 800 °C (Fig. 3), particularly for the $LaCoO_3$ and $La_{0.8}Ca_{0.2}CoO_3$ compositions.

The notable exception, like in Fig. 4, is in the case of $La_{0.45}Ca_{0.55}CoO_3$ where significantly higher ($2.2 \pm .11$ MPa $m^{1/2}$) fracture toughness was observed. This composition is known to be non-stoichiometric with significant amounts of secondary phases (CaO and CoO), and thus at high temperatures oxidation of CoO to Co_3O_4 and the resulting plastic deformation could influence the fracture toughness values [33]. Fig. 7 also indicates a predominantly intergranular crack propagation for all 4 compositions at 800 °C, which is a characteristic feature of high temperature crack propagation [33].

3.5. Compression behavior

Ferroelastic hysteresis loops obtained during uniaxial compression of the four perovskites are shown in Fig. 8. For the same maximum stress and loading rate, each of the four cobaltite compositions exhibited different ferroelastic behavior, such as different inflection points, hysteresis areas and maximum strain. For the undoped $LaCoO_3$ (Fig. 8a), a significant softening of the stress–strain deformation started at 25–30 MPa and the inflection point was reached at 66 MPa. A hardening in the stress–strain response was observed when the stress value increased beyond the inflection point. For $La_{0.8}Ca_{0.2}CoO_3$ (Fig. 8b) the coercive stress was found to be at a much higher stress of 130 MPa with a larger hysteresis loop area as compared to $LaCoO_3$. For the two non-stoichiometric compositions, $La_{0.6}Ca_{0.4}CoO_3$ and $La_{0.45}Ca_{0.55}CoO_3$ (Fig. 8c and d), the inflection point was found to be around ~270 MPa. Note that these two compositions show a similar shape and area of their hysteresis curves. This can be attributed to the precipitation of the secondary phases such as CaO and CoO in these compounds, which has a significant influence on their behavior during compression. A further detailed study is currently underway in order to determine the effects of repeated loading on the hysteresis behavior of the cobaltites.

3.6. Conductivity

The electronic conduction in pure $LaCoO_3$ occurs by transfer of charge carriers via Co–O–Co bonds. As already reported in [21,34,35], $LaCoO_3$ exhibits an unusual thermally activated conductivity characterized as a small polaron hopping conductivity at room temperature [35,36], but showing a dramatic increase in electrical conductivity in the temperature range 300–500 °C. At temperatures above 320–350 °C a metallic phase containing high-spin Co^{3+} and intermediate spin Co (1 1 1) ions is stabilized and the partially filled σ_α^* band is responsible for the p-type conductivity [37].

The electrical conductivities of the four cobaltite compositions are presented in Fig. 9. At 750 and 900 °C, the conductivity of $LaCoO_3$ is measured to be 920 and 898 S cm^{-1} respectively (Fig. 9), which corresponds well to the reported values of ~1000 S cm^{-1} above 725 °C [21]. Based on the reported increase in conductivity, the semiconductor-to-metal transition has been proposed to occur in $LaCoO_3$ in this temperature range, due to a gradual transition involving the thermal promotion of electrons from a π^* band associated with the localized t_{2g} orbitals to a delocalized σ^* band associated with the e_g orbitals [38]. The reported activation energy of the semiconductor-to-metallic transition is about 0.11 eV [39]. The semiconductor-to-metallic transition in $LaCoO_3$ can also be detected by Raman spectroscopy, where two bands present in the semiconducting state disappear upon heating above 230 °C,

accompanied by a significant drop in resistivity [14,40]. Neutron-scattering measurements show that the semiconductor-to-metal crossover behavior has no magnetic origin [41]. The high temperature metallic state in $LaCoO_3$ has been reported to have an electronic structure very similar to that of a doping induced metallic state in $La_x(Sr\text{ or }Ca)_{1-x}CoO_3$ [10,20].

The electrical resistivities of 20 mol% Ca substituted $LaCoO_3$, along with results on 10, 12 and 15 mol% Ca substitution, measured at room temperature and below have been reported in [42]. Doping of pure $LaCoO_3$ with Ca^{2+} ions on the A site generates a charge disproportionation of Co^{3+} to Co^{4+} with a simultaneous deviation from the oxygen stoichiometry, and an extensive formation of oxygen vacancies are expected. It has been pointed out [43] that partial substitution of La^{3+} by divalent alkaline-earth metals will bring forth the formation of more low spin Co^{4+} ($t_{2g}^5 l_g^0$) ions and stabilize the neighboring Co^{3+} ions in intermediate spin state ($t_{2g}^5 l_g^1$). Such doping results in the significant decrease in the activation energy (ε_p) for p-type conductivity from $\varepsilon_p = 0.132$ eV for $LaCoO_3$ to $\varepsilon_p = 0.044$ eV for $La_{0.8}Ca_{0.2}CoO_3$. Consequently, a significant increase both in room and high temperature conductivity of $La_{0.8}Ca_{0.2}CoO_3$ is observed (Fig. 9). The maximum conductivity of ~1770 S cm^{-1} for $La_{0.8}Ca_{0.2}CoO_3$ was measured in 200–300 °C temperature range with slight decrease in conductivity to ~1400 S cm^{-1} at 800–900 °C, which is in good agreement with reported data. Since the limit of the solid solubility of Ca^{2+} lies in the region of 0.28 at% [13], the compositions with 40 and 55% Ca doping exhibit the formation (precipitation) of the secondary phases, such as CaO and Co_3O_4. The resulting $La_{0.6}Ca_{0.4}CoO_3$ and $La_{0.45}Ca_{0.55}CoO_3$ compositions are not phase pure and, while

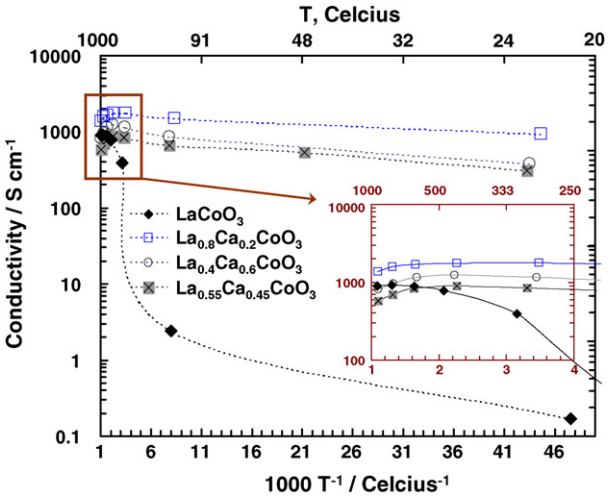

Fig. 9. Comparison of the conductivities of the cobaltites from room temperature to 900 °C.

they still exhibit fairly good electrical conductivity at 300–500 °C (Fig. 9), their room temperature conductivity (~375 S cm^{-1} for $La_{0.6}Ca_{0.4}CoO_3$ and ~300 S cm^{-1} for $La_{0.45}Ca_{0.55}CoO_3$ at 27 °C) is not as high as those of phase pure $La_{0.8}Ca_{0.2}CoO_3$ (Fig. 9). Note that although $La_{0.8}Ca_{0.2}CoO_3$ demonstrates the best electronic conductivity amongst the compositions tested in this work, all of the four compositions possess adequate conductivity (>170 S cm^{-1} [44]) for potential use in IT-SOFCs. Further studies in this respect should

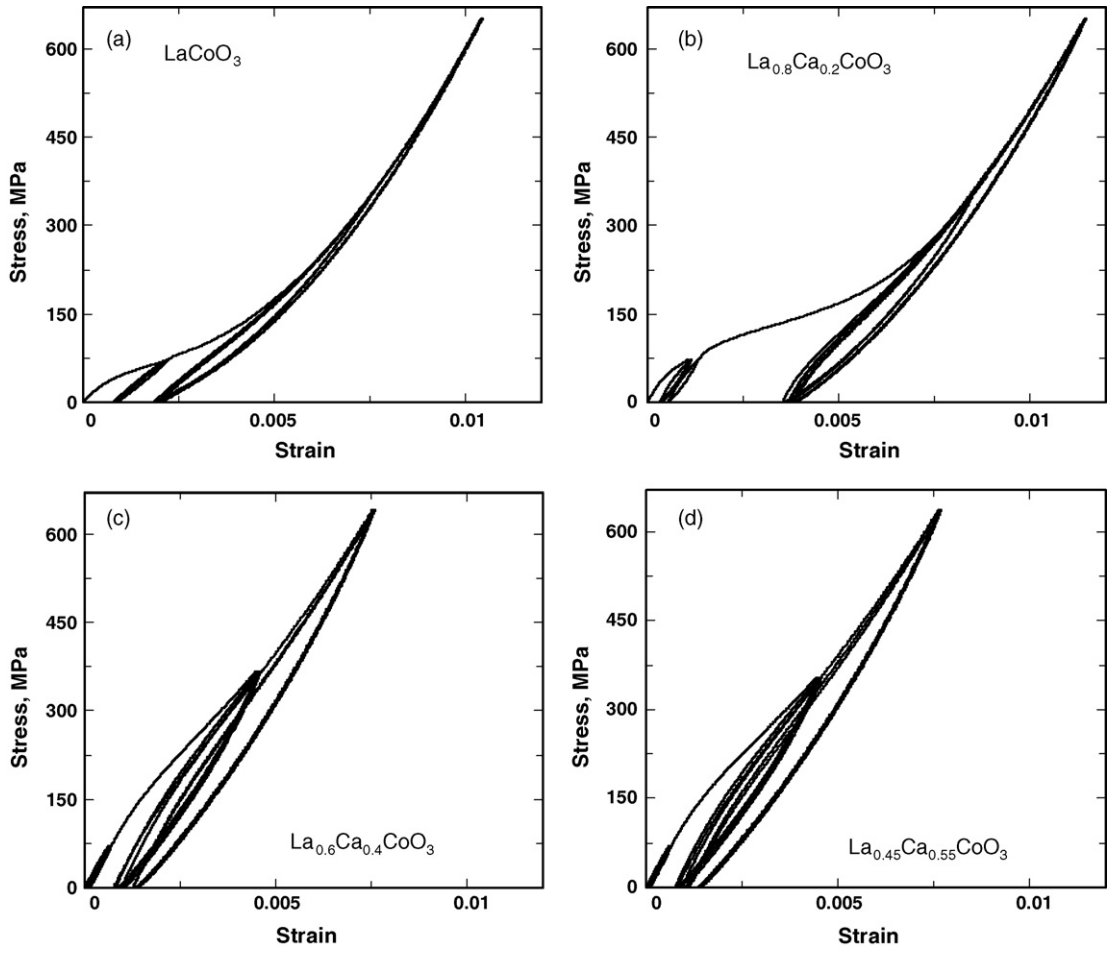

Fig. 8. Stress–strain behavior for the four cobaltite compositions during compression at room temperature.

concentrate on other factors – such as the cathodic interfacial polarization resistance of the cobaltites at IT-SOFC operating temperatures, as well as their chemical stability and thermal expansion coefficient mismatch with the electrolyte – which are also likely to influence their selection for applications in IT-SOFCs.

4. Conclusions

In this work we have summarized the mechanical behavior and electrical conductivities of four $LaCoO_3$ based cobaltite compositions; two-phase pure materials ($LaCoO_3$ and $La_{0.8}Ca_{0.2}CoO_3$), and two compositions with secondary phases present ($La_{0.6}Ca_{0.4}CoO_3$ and $La_{0.45}Ca_{0.55}CoO_3$). At room temperature, the undoped $LaCoO_3$ composition demonstrates a lower Young's modulus value (~60–70 GPa), with significant stiffening observed for the Ca doped compositions (modulus 130–140 GPa). The opposite tendency was noted for the samples tested at 800 °C, where the pure $LaCoO_3$ became more stiff (modulus 101 GPa), but the $La_{0.8}Ca_{0.2}CoO_3$ perovskite exhibited a significant softening (modulus 65 GPa).

For the phase pure compositions, the trends in the modulus values were reflected in the four-point bending and fracture toughness test results. At room temperature, the undoped $LaCoO_3$ exhibited the lowest strength of 72 ± 10 MPa, with the three Ca^{2+} doped compositions exhibiting higher strengths of ~180 MPa. The strength values for $LaCoO_3$ were found to increase (to 109 ± 19 MPa) at 800 °C, and this high temperature value remained more or less constant with increase in Ca^{2+} doping of up to 40% Ca. Similarly the Ca^{2+} doped compositions were found to have a higher K_{Ic} value than the undoped $LaCoO_3$ at room temperature, followed by a decrease in fracture toughness for the $La_{0.8}Ca_{0.2}CoO_3$ and $La_{0.6}Ca_{0.4}CoO_3$ compositions at 800 °C. The very high strength and fracture toughness values for the $La_{0.45}Ca_{0.55}CoO_3$ composition at 800 °C was probably caused by the secondary phases present in this composition at this elevated temperature.

All of the four compositions exhibited ferroelastic behavior, as confirmed by the hysteresis loops generated during uniaxial load–unload compression tests. The coercive stress values calculated from these tests were found to increase with increase in Ca^{2+} doping (σ_c = 66 MPa for pure $LaCoO_3$, 130 MPa for 20% Ca^{2+} doped, and ~270 MPa for both 40 and 55 mol% Ca^{2+} doped). The stress–strain behavior for the 40 and 55 mol% Ca^{2+} doped compositions were also found to be remarkably similar. Electrical conductivity results showed the 20 mol% Ca^{2+} doped composition to have the maximum value, where a significant amount of mobile defects are generated due to substitution of La^{3+} ions for the divalent Ca^{2+} ions. The pure $LaCoO_3$ composition was also seen to exhibit the well known semiconductor-to-metal transition behavior upon heating.

In summary this work found the 20 mol% Ca^{2+} doped cobaltite composition to be the most promising for both mechanical and electrical performance across the range of temperatures for IT-SOFC applications tested in this work.

Acknowledgements

The authors would like to thank Mr R. Bächtold for their help in performing the mechanical tests, and Ms. Laura Fagely for her assistance in the XRD measurements. This research was supported by the National Science Foundation NSF, DMR (project #0201770). This research was also supported in part by the 2005 Southeastern Universities Research Association (SURA) – Oak Ridge National Laboratory (ORNL) Summer Cooperative Research Program Scholarship, and the Thesis grant from EMPA, Duebendorf, Switzerland. Research at the Oak Ridge National Laboratory's High Temperature Materials Laboratory was sponsored by the U.S. Department of Energy, Office of Energy Efficiency and Renewable Energy, Vehicle Technologies Program.

References

[1] M. Feng, J.B. Goodenough, K. Huang, C. Milliken, Journal of Power Sources 63 (1996) 47–51.
[2] U. Balachandran, J.T. Dusek, S.M. Sweeney, R.B. Poeppel, R.L. Mieville, P.S. Maiya, M.S. Kleefisch, S. Pei, T.P. Kobylinski, C.A. Udovich, American Ceramic Society Bulletin 74 (1995) 71–75.
[3] K. Huang, M. Feng, J.B. Goodenough, M. Schmerling, Journal of the Electrochemical Society 143 (1996) 3630–3636.
[4] F. Tietz, Ionics 5 (1999) 129–139.
[5] S. Uhlenbruck, F. Tietz, Materials Science and Engineering B (2004) 277–282.
[6] N. Orlovskaya, Y. Gogotsi, M. Reece, B. Cheng, I. Gibson, Acta Materialia 50 (2002) 715–723.
[7] Y. Kobayashi, T. Mitsunaga, G. Fujinawa, T. Arii, M. Suetake, K. Asai, J. Harada, Journal of the Physical Society of Japan 69 (2000) 3468–3469.
[8] N. Orlovskaya, M. Lugovy, S. Pathak, D. Steinmetz, J. Lloyd, L. Fegely, M. Radovic, E.A. Payzant, E. Lara-Curzio, L.F. Allard, J. Kuebler, Journal of Power Sources 182 (2008) 230–239.
[9] A. Mineshige, M. Inaba, T. Yao, Z. Ogumi, K. Kikuchi, M. Kawase, Journal of Solid State Chemistry 121 (1996) 423–429.
[10] P. Ravindran, P.A. Korzhavyi, H. Fjellvåg, A. Kjekshus, Physical Review B 60 (1999) 16423–16434.
[11] R. Caciuffo, D. Rinaldi, G. Barucca, J. Mira, J. Rivas, M.A. Señarís-Rodríguez, P.G. Radaelli, D. Fiorani, J.B. Goodenough, Physical Review B 59 (1999) 1068–1078.
[12] K. Asai, A. Yoneda, O. Yokokura, J.M. Tranquada, G. Shirane, K. Kohn, Journal of the Physical Society of Japan 67 (1998) 290–296.
[13] J. Mastin, M.A. Einarsrud, T. Grande, Chemistry of Materials 18 (2006) 1680–1687.
[14] N. Orlovskaya, D. Steinmetz, S. Yarmolenko, D. Pai, J. Sankar, J. Goodenough, Physical Review B (Condensed Matter and Materials Physics) 72 (2005) 14122-1–14122-7.
[15] G. Maris, Y. Ren, V. Volotchaev, C. Zobel, T. Lorenz, T.T.M. Palstra, Physical Review B (Condensed Matter and Materials Physics) 67 (2003) 224423-1–224423-5.
[16] P.E. Vullum, R. Holmestad, H.L. Lein, J. Mastin, M.A. Einarsrud, T. Grande, Advanced Materials 19 (2007) 4399–4403.
[17] P.E. Vullum, H.L. Lein, M.A. Einarsrud, T. Grande, R. Holmestad, Philosophical Magazine 88 (2008) 1187–1208.
[18] M.A. Korotin, S.Y. Ezhov, I.V. Solovyev, V.I. Anisimov, D.I. Khomskii, G.A. Sawatzky, Physical Review B (Condensed Matter) 54 (1996) 5309–5316.
[19] V.V. Kharton, E.N. Naumovich, A.V. Kovalevsky, A.P. Viskup, F.M. Figueiredo, I.A. Bashmakov, F.M.B. Marques, Solid State Ionics, Diffusion & Reactions 138 (2000) 135–148.
[20] Y. Tokura, Y. Okimoto, S. Yamaguchi, H. Taniguchi, T. Kimura, H. Takagi, Physical Review B (Condensed Matter) 58 (1998) 1699–1702.
[21] S.R. Sehlin, H.U. Anderson, D.M. Sparlin, Physical Review B 52 (1995) 11681.
[22] K. Kleveland, N. Orlovskaya, T. Grande, A.M.M. Moe, M.-A. Einarsrud, K. Breder, G. Gogotsi, Journal of the American Ceramic Society 84 (2001) 2029–2033.
[23] N. Orlovskaya, K. Kleveland, T. Grande, M.-A. Einarsrud, Journal of the European Ceramic Society 20 (2000) 51–56.
[24] European Standard, EN 623-2, Advanced Technical Ceramics – Monolithic Ceramics – General and Textural Properties. Part 2. Determination of Density and Porosity, Sep 1993.
[25] R. Rosten, M. Koski, E. Koppana, Journal of Undergraduate Research 2 (2006) 38–41.
[26] peEN 843-2, Methods of Test for Advanced Technical Ceramics – Review of ENV 843-2. Determination of Elastic Moduli at Room Temperature. Feb 2004.
[27] J. Kübler. Fracture Toughness of Ceramics Using the SEVNB Method: From a Preliminary Study to a Standard Test Method, Fracture Resistance Testing of Monolithic and Composite Brittle Material, 2002.
[28] ASTM Designation: F 43-93, Standard Test Methods for Resistivity of Semiconductor Materials, Oct 1993.
[29] M. Radovic, E. Lara-Curzio, L. Riester, Materials Science & Engineering A (Structural Materials: Properties, Microstructure and Processing) A368 (2004) 56–70.
[30] A.R. Boccaccini, Z. Fanb, Ceramics International 23 (1997) 239–245.
[31] E.A. Dean, J.A. Lopez, Journal of the American Ceramic Society 66 (1983) 366–370.
[32] A. Selçuk, A. Atkinson, Journal of the European Ceramic Society 17 (1997) 1523–1532.
[33] D. Munz, G. Himsolt, J. Eschweiler, in: S.W. Freiman, E.R. Fuller (Eds.), Fracture Mechanics Methods for Ceramics, Rocks, and Concrete, ASTM STP 745, American Society for Testing and Materials, Philadelphia, PA, USA, 1981, pp. 69–84.
[34] C.S. Naiman, R. Gilmore, B. DiBartolo, A. Linz, R. Santoro, Journal of Applied Physics 36 (1965) 1044–1045.
[35] P.M. Raccah, J.B. Goodenough, Physical Review 155 (1967) 932–942.
[36] H.G. Reik, E. Kauer, P. Gerthsen, Physics Letters 8 (1964) 29–30.
[37] M.A. Senaris-Rodriguez, J.B. Goodenough, Journal of Solid State Chemistry 118 (1995) 323–336.
[38] G. Thornton, I.W. Owen, G.P. Diakun, Journal of Physics: Condensed Matter 3 (1991) 417–422.

[39] S. Yamaguchi, Y. Okimoto, H. Taniguchi, Y. Tokura, Physical Review B (Condensed Matter) 53 (1996) 2926–2929.
[40] D.P. Kozlenko, N.O. Golosova, Z. Jirak, L.S. Dubrovinsky, B.N. Savenko, M.G. Tucker, Y. Le Godec, V.P. Glazkov, Physical Review B (Condensed Matter and Materials Physics) 75 (2007) 64422-1–64422-10.
[41] K. Asai, O. Yokokura, N. Nishimori, H. Chou, J.M. Tranquada, G. Shirane, S. Higuchi, Y. Okajima, K. Kohn, Physical Review B (Condensed Matter) 50 (1994) 3025–3032.
[42] J. Yi, H. Kong, C. Zhu, Journal of Alloys and Compounds 474 (2009) 38–41.
[43] D. Louca, J.L. Sarrao, Physical Review Letters 91 (2003) 155501.
[44] W. Gong, S. Gopalan, U.B. Pal, Journal of the Electrochemical Society 152 (2005) A1890–A1895.